Energy & Environmental Science

PAPER

View Article Online
View Journal | View Issue

Cite this: *Energy Environ. Sci.*, 2017, **10**, 1828

The role of iodide in the formation of lithium hydroxide in lithium–oxygen batteries†

Michał Tułodziecki,*[a] Graham M. Leverick,[b] Chibueze V. Amanchukwu,[c] Yu Katayama,[bd] David G. Kwabi,[b] Fanny Bardé,[e] Paula T. Hammond[c] and Yang Shao-Horn*[abf]

Received 7th April 2017,
Accepted 17th July 2017

DOI: 10.1039/c7ee00954b

rsc.li/ees

Lithium iodide has been studied extensively as a redox-mediator to reduce the charging overpotential of Li–oxygen (Li–O_2) batteries. Ambiguities exist regarding the influence of lithium iodide on the reaction product chemistry and performance of lithium–oxygen batteries. In this work, we examined the role of lithium iodide on the reduction product chemistry under two conditions: (i) mixing KO_2 with lithium salts and (ii) discharging Li–oxygen batteries at high and low overpotentials, in the presence of an ether-based electrolyte with different ratios of H_2O : LiI. The addition of iodide to electrolytes containing water was found to promote the formation of LiOOH·H_2O, LiOH·H_2O and LiOH at the expense of Li_2O_2. At low H_2O : LiI ratios (lower than 5), LiOH instead of Li_2O_2 was formed, which was accompanied by the oxidation of iodide to triodide while at high H_2O : LiI ratios (12, 24, 134), a mixture of Li_2O_2, LiOOH·H_2O and LiOH·H_2O was observed and no triiodide was detected. The reaction between peroxide Li_2O_2 and/or superoxide LiO_2 with H_2O to form LiOH is facilitated by increased water acidity by strong I^-–H_2O interactions as revealed by ^{1}H NMR and FT-IR measurements. This mechanism of LiOH formation in the presence of LiI and H_2O was also found upon Li–O_2 cell discharge, which is critical to consider when developing LiI as a redox mediator for Li–O_2 batteries.

Broader context

Lithium–air batteries can potentially offer three times the gravimetric energy of commercial Li-ion batteries. Unfortunately, the poor reversibility and kinetics of lithium–oxygen (Li–O_2) chemistry in aprotic electrolytes remains a critical challenge that limits their practical use. Redox mediators such as lithium iodide (LiI) have been shown to lower the charging overpotential and improve cycle life. Ambiguities exist in terms of the effect of LiI on the reversibility of electrochemical reduction of oxygen in the presence of lithium ions (Li^+, O_2 redox chemistry) and battery cyclability. Some studies have shown high reversibility of Li–oxygen chemistry with LiI upon prolonged cycling while others report poor reversibility and efficiency due to the formation of LiOH. The role of iodide and mechanistic details regarding the formation of LiOH are not understood, which is critical to assess if LiI can be used as a redox mediator to promote the kinetics of Li–O_2 batteries. We show that LiI can increase the acidity of H_2O and facilitate the deprotonation of H_2O by strong oxidants such as Li_2O_2 and/or LiO_2 formed from chemical disproportionation or lithium–oxygen battery discharge, which promotes the formation of LiOH instead of Li_2O_2 in an ether-based electrolyte. Increasing the H_2O : LiI ratios can decrease H_2O acidity and change the products from LiOH to a mixture of Li_2O_2, LiOOH·H_2O and LiOH·H_2O. Therefore, strategies to suppress the deprotonation of water and electrolyte solvents are needed to prevent LiOH formation in the presence of LiI and increase the reversibility and performance of Li–O_2 batteries.

[a] *Research Laboratory of Electronics, Massachusetts Institute of Technology, 77 Massachusetts Avenue, Cambridge, Massachusetts 02139, USA. E-mail: michalt@mit.edu, shaohorn@mit.edu*
[b] *Department of Mechanical Engineering, Massachusetts Institute of Technology, 77 Massachusetts Ave, Cambridge, MA 02139, USA*
[c] *Department of Chemical Engineering, Massachusetts Institute of Technology, 77 Massachusetts Ave, Cambridge, MA 02139, USA*
[d] *Department of Energy and Hydrocarbon Chemistry, Graduate School of Engineering, Kyoto University, Kyoto 615-8510, Japan*
[e] *Research & Development 3, Advanced Technology 1, Toyota Motor Europe, Hoge Wei 33 B, B-1930 Zaventem, Belgium*
[f] *Department of Materials Science and Engineering, Massachusetts Institute of Technology, 77 Massachusetts Ave, Cambridge, MA 02139, USA*
† Electronic supplementary information (ESI) available. See DOI: 10.1039/c7ee00954b

Introduction

Lithium–oxygen (Li–O_2) batteries have received much attention during the past decade due to their high theoretical specific energy (3500 W h kg^{-1} at the cell level)[1] which is three times higher than that of the current commercial Li-ion batteries based on $LiCoO_2$ active material (1000 W h kg^{-1}). The mechanism of Li–O_2 batteries is based on a different principle than Li-ion batteries; namely instead of intercalation of Li^+ into a metal oxide host, lithium ions react with reduced oxygen species to form Li_2O_2 deposits inside a porous cathode matrix.[2]

In practice, the specific energy is limited by the capability of the cathode material to accommodate large quantities of Li_2O_2. One of the main problems related to Li_2O_2 precipitation is its insulating nature. The Li_2O_2 precipitate passivates the electrode surface hindering further electron transfer.[3,4] This obstacle can be overcome, to some extent, by designing high surface area structures of the carbon matrix,[2,5] and modifying the surface chemistry[6] and the morphology of the deposited Li_2O_2.[7–10] However, the insulating nature of Li_2O_2 brings further complications during the charge process. In particular, the sluggish kinetics of charge transfer result in high charging over potentials, low rate capability, low energy efficiency, numerous parasitic reactions and poor cycle life.[1,2,11,12]

In addition to the use of solid-state catalysts[13–15] such as metal oxides,[16,17] modified carbon,[18–20] or metals[8,21] and their alloys[22] to mitigate sluggish reaction kinetics, soluble redox mediators have been shown recently to promote the kinetics of charge transfer through chemical oxidation of Li_2O_2 rather than direct electrochemical oxidation.[23–34] In the electrochemical step, the soluble redox mediator is oxidized (reaction (1)), following which it chemically reacts with Li_2O_2 (reaction (2)).

$$RM \rightleftharpoons RM_{(soluble)}^{+} + e^{-} \quad (1)$$

$$Li_2O_{2(solid)} + 2RM_{(soluble)}^{+} \rightleftharpoons RM + O_2 + 2Li^{+} \quad (2)$$

Because of the solvation of the mediator, the second step does not need to occur at the electrode surface; an oxidized mediator can access the Li_2O_2 precipitate that is not in direct contact with an electrode. Such mechanisms have already been shown to lower the charging overpotentials and consequently, greatly improve the energy efficiency of Li–O_2 batteries.[23–31,33,34] A variety of redox mediators have been studied: tetrathiofulvalene (TTF),[27,28] tris[4-(diethylamino)phenyl]amine (TDPA),[24] 2,2,6,6-tetramethylpiperidinyloxyl (TEMPO),[29,30] 10-methylphenothiazine (MPT),[31] phthalocyanine (FePc),[23] iodide (I^-)[25,32,34,35] and bromide (Br^-).[33,36]

LiI has been studied intensively to decrease charging overpotential and improve the cycle life of Li–O_2 batteries.[25,32,34,35,37] Ambiguities exist in terms of its effect on the reversibility, cyclability, and reaction mechanism of lithium–oxygen redox chemistry.[26,32,38–40] For example, Lim *et al.*[34] reported an oxidation plateau at 3.3 V up to 900 cycles using carbon nanotubes and tetraethylene glycol dimethyl ether (TEGDME) with 0.05 M LiI. Liu *et al.*[35] have reported oxidation potentials lower than 3.2 V for 3000 cycles using reduced graphene and an electrolyte based on water-containing DME (45 000 ppm of H_2O) with 0.05 M LiI. This performance has been attributed to a reaction mechanism involving the formation of LiOH *via* $O_2 + 4Li^+ + 2H_2O + 4e^- \rightleftharpoons 4LiOH$ on discharging and consumption of LiOH by triiodide formed at voltages lower than 3.2 V_{Li} on charging *via* $4LiOH + 2I_3^- \rightleftharpoons 4Li^+ + O_2 + 2H_2O + 6I^-$. However, UV-Vis experiments by Shen *et al.*[39] and the analysis of reaction free energies by Viswanathan *et al.*[40] show that the reversible LiOH oxidation by triiodide is unlikely. Most recently, Zhu *et al.*[32] have reported that a mixture of $LiOOH{\cdot}H_2O$ and $LiOH{\cdot}H_2O$ is formed during discharge while on charging the $LiOOH{\cdot}H_2O$ is oxidized by I_3^- and $LiOH{\cdot}H_2O$ by I_2 species in DME-based electrolytes with high water content (>100 000 ppm) similar to the results reported by Liu *et al.*[35] These findings are different from those of Burke *et al.*,[38] where LiOH was formed upon Li–O_2 battery discharge with H_2O (5000 ppm) and 0.2 M LiI in DME. In addition, this work shows low efficiency of triiodide for the oxidation of Li_2O_2 into oxygen in DME-based electrolytes[38] in contrast to other studies[25,26,34,35,37] and neither I_3^- nor I_2 can oxidize LiOH from DEMS and iodometric titration measurements. These authors instead suggest that LiOH can react with I_2 during charging to form soluble $LiIO_3$ ($3I_2 + 6LiOH \rightleftharpoons LiIO_3 + 5LiI + 3H_2O$), which is irreversible during subsequent cycles. These observations are supported by Kwak *et al.*,[26] where fast deterioration in the energy efficiency of Li–O_2 batteries cycled with 0.05 M LiI solution in TEGDME (H_2O <10 ppm) and carbon paper has been attributed to the irreversible formation of LiOH from deprotonation of TEGDME, rather than H_2O, by Li_2O_2 which is mediated by iodide ions. Therefore, further understanding the role of iodide in the formation and oxidation of LiOH is much needed and critical to assess if LiI can be used as a redox mediator to promote the kinetics of Li–oxygen batteries.

In this study, we focus on examining the role of iodide in the formation of LiOH under two experimental conditions: (i) reacting KO_2 with lithium salts in DME solution and (ii) the electrochemical reduction of Li^+–oxygen in lithium–oxygen batteries at high potentials (~2.7 V), where Li_2O_2 is formed largely by disproportionation of LiO_2, and at low potentials (~2.2 V), where Li_2O_2 is formed directly through electrochemical steps.[41] In these experiments, the addition of H_2O to the DME-based electrolyte (typically containing around 40 ppm of H_2O) as a proton source for LiOH formation is studied. The solid reaction products are probed by Raman spectroscopy, ^1H NMR and X-ray diffraction while the liquid phase is examined by UV-Vis and ^1H NMR spectroscopy. The oxidation of iodide to triiodide in these measurements is quantified using UV-Vis spectroscopy and iodometric titration. In the absence of substantial H_2O (40 ppm H_2O) in the electrolyte, chemical disproportionation (in the presence of KO_2 with lithium salts) and electrochemical reduction of Li^+–O_2 at both high and low discharge voltages result in the formation of mostly Li_2O_2, regardless of the presence of LiI. On the other hand, the addition of LiI changed the main product from Li_2O_2 to LiOH in electrolytes with low H_2O : LiI ratios (up to 5), which is accompanied by the oxidation of I^- to I_3^- for chemical reactions and electrochemical reactions at low overpotentials. The addition of LiI in the electrolytes with high H_2O : LiI molar ratios greater than 5 leads to a mixture of Li_2O_2, $LiOOH{\cdot}H_2O$ and $LiOH{\cdot}H_2O$. These different products observed can be explained by the hypothesis that the reactions between peroxide Li_2O_2 and/or superoxide LiO_2 with H_2O to form LiOH can be facilitated by increased water acidity by strong I^-–H_2O interactions as revealed by ^1H NMR and FT-IR.

Experimental

Chemicals

High purity dimethyl sulfoxide was purchased from Sigma Aldrich (99.9% pure anhydrous). DME was purchased from

Acros and was degassed and dried using a Glass Contour Solvent Purification System built by SG Water USA, LLC. The solvents were further dried over molecular sieves for at least one week before use. Lithium bis(trifluoromethanesulfonyl)imide (from Nippon Shokubai) was dried at 160 °C under vacuum for 24 hours. High purity LiI (99.999% pure), KI (99.998% pure), I_2 (99.999% pure) and Li_2O_2 (90%) chemicals were ordered from Alfa Aesar and were used as received. The starting Li_2O_2 powder sample contains LiOH and Li_2CO_3 impurities estimated at ~13% and ~1%, respectively, from the XRD data.[42] KO_2 (99% pure) powder was purchased from Sigma Aldrich and was used as received. All chemicals were stored in an argon-filled glovebox with H_2O and O_2 contents <0.1 ppm. The electrolytes were prepared by dissolution of a desired amount of salts in the solvent. The total H_2O content in the solvents and electrolytes was checked using a C30 compact Karl Fisher coulometer from Mettler Toledo and for the dry solvent it was <10 ppm for ~2 g of the test sample. The solution containing lithium salts (0.2 M LiI plus 0.1 M LiTFSI) had a slightly higher water content of 40 ppm, coming from residual water in the salts. Electrolytes containing a high amount of water (from 1000 to 146 000 ppm of H_2O) were prepared by adding deionized water (18.2 MΩ cm, Millipore) to the dry solvents outside the glove box. Next, the obtained solvent was extensively bubbled with argon gas inside the glovebox for 15 min in order to remove all of the oxygen. The H_2O content was confirmed using the Karl Fisher coulometer.

The effect of iodide ions on lithium peroxide formation was studied using a chemical route. KO_2 powder was added to solutions with varied H_2O content (from 40 ppm to 146 000 ppm) and type of Li salt (LiI or LiTFSI). The reaction between Li^+ and KO_2 (disproportionation reaction (3))[2]

$$2O_2^- + 2Li^+ \rightarrow Li_2O_2 + O_2 \quad (3)$$

is very fast and results in O_2 evolution and precipitation of a white powder in all the studied samples. The molar ratio of KO_2 to Li^+ ions (1 : 3) was kept constant in all of the samples, while the total concentration of Li^+ in each solution was 0.3 M, unless otherwise specified. Thus, assuming 100% efficiency, the total possible amount of produced Li_2O_2 is 50 mM. If not otherwise specified, the resultant precipitate was separated from the liquid phase by centrifugation/decantation, and further washed 3 times with dry solvent in order to remove residual salt. The duration of each reaction is indicated in the figure captions. The precipitate was studied by Raman spectroscopy and ^{1}H NMR (using D_2O as co-solvent), while the liquid phase was examined by UV-Vis and ^{1}H NMR (using deuterated DMSO as co-solvent) spectroscopy.

The presence of H_2O_2-like species was detected by Quantofix strips purchased from Sigma Aldrich. The strips are sensitive to the presence of hydrogen peroxide, peracetic acid and different organic/inorganic hydroxyperoxides. The detection mechanism is based on the peroxidase compound and organic redox indicators.[43]

Solutions with oxygen atmosphere were prepared by bubbling the solution with O_2 for 20 minutes and sealing the sample afterwards.

Battery assembly

The Li–O_2 cells consisted of a lithium metal anode and free-standing vertically aligned few-walled CNTs (detailed preparation of the nanotubes has been previously reported[44,45]) as the O_2 electrode (~1 × 1 $cm^2_{geo.}$). After weighing and vacuum-drying at 100 °C for 8 hours, the electrodes were transferred to a glove box (H_2O <0.1 ppm, O_2 <0.1 ppm, Mbraun, USA) without exposure to ambient air. The carbon loadings were on average 1.6 mg $cm^{-2}_{geo.}$. The cells were assembled with a lithium foil anode (Chemetall, Germany, 15 mm in diameter) and soaked in 150 μl of electrolyte. A 316 stainless steel mesh was used as the current collector. The cathode and anode were separated by 2 Celgard 2325 separators. Following assembly, the cells were transferred to a connected second argon glove box (Mbraun, USA, H_2O <1 ppm, O_2 <1%) without exposure to air and pressurized with dry O_2 (99.994% pure O_2, Airgas, H_2O <2 ppm) to 25 psi (gauge) to ensure that an adequate amount of O_2 was available. The oxygen pressure in the cell was measured using a pressure gauge during the experiments to confirm proper cell sealing. Electrochemical tests were conducted using a Biologic VMP3. All discharge tests were performed by first resting at open circuit (~2.9–3.2 V_{Li}) for 6 hours. Three different discharge conditions were used (i) potentiostatic discharge at 2.7 V_{Li}, (ii) galvanostatic discharge at 12.5 mA g^{-1} and (iii) potentiostatic discharge at 2.2 V_{Li}.

Characterization

UV-Vis was performed using a Beckman Coulter DU 800 spectrophotometer. The pure solvent (*e.g.* DME) was used as the blank solution. Solutions were prepared in an argon glovebox and sealed in a quartz cuvette used for data collection, preventing air exposure. Due to the high molar absorptivity of I_3^-, the solutions with I_3^- were diluted so that the intensity of the I_3^- absorption signals (at 293 nm and 364 nm) was within the calibration range (Fig. S2, ESI†). The concentrations of triiodide were calculated based on the absorption intensity of both the 293 and 364 nm signals by averaging the value, unless one of the absorbance peaks was out of the calibration range, in which case only one wavelength was used. The very high molar absorptivity (52341 dm^3 (mol cm)$^{-1}$ at 293 nm and 27 054 dm^3 (mol cm)$^{-1}$ at 364 nm) of triiodide in DME allows for the detection of I_3^- concentrations as low as 0.002 mM. The absorption spectra in the figures are rescaled (arbitrary units) in order to visualize the difference in I_3^- concentration for different solutions. Thus, a high concentration of I_3^- corresponds to high absorption at wavelengths 293 nm and 364 nm and *vice versa*. The scale factors and the calculation of I_3^- concentrations are summarized in Table S1 (ESI†). For solution preparation and dilution, the same micropipettes were used (1 ml, 0.1 ml and 0.02 ml), the pipette tips were first wetted 2 times with the desired solution by slowly aspirating and dispensing it. In all cases the pipetted volumes were greater than 50% of the maximum pipette volume in order to maximize accuracy. The I_3^- concentration measurement error comes mostly from the pipetting procedure that varies depending on

the number of dilutions and is estimated to be 1%, 2% and 3% for 1, 2 and 3 dilutions, respectively.

Iodometric titration was performed with 0.01 M thiosulfate (anhydrous 99.99% Sigma-Aldrich, stored in desiccator) using a 50 ml burette (Class A, graduation 0.10 ml, tolerance ±0.05 ml from VWR) and starch indicator (1% w/v of Amylodextrin) in aqueous solution (Ricca Chemical). The thiosulfate solution was first standardized with KIO_3 (99.995% pure from Sigma Aldrich) solution of a known concentration (2.3 mM) in three separate probes. 10 ml of KOI_3 solution was added to an Erlenmeyer flask (250 ml), to which 100 mg of KI (Bioultra >99.5% TA from Sigma Aldrich) and 4 ml of 6 M H_2SO_4 were added. The obtained I_3^- solution was immediately titrated with thiosulfate solution. Just before the end-point, indicated by a light straw-like color, the starch solution was added, resulting in a change of color to dark red/brown (this color change is due to branched Amylodextrin rather than blue when using straight chain amylose). The quantification of triiodide in the electrolyte samples was done by mixing 1 ml of sample in 5 ml of H_2O containing 50 mg of KI, and titrating with standardized thiosulfate solution as described above. The thiosulfate solution was prepared fresh the same day as the titration experiment. Verification of the experimental procedure was done by titrating known concentrations of triiodide in DME prepared by mixing lithium iodide and iodine in DME (50.7 mM and 24.9 mM). Averaged concentrations of 50.5 and 24.8 mM were found from 2 independent probes, confirming the accuracy of the titration method. The estimated I_3^- concentration error, based on the burette tolerance of ±0.05 ml, is ±0.3 mM.

Raman spectroscopy was performed on a LabRAM HR800 microscope (Horiba Jobin Yvon) using an external 20 mW He:Ne 633 nm laser (Horiba, Jobin Yvon), focused with a 50× long working distance objective and a $10^{-0.3}$ neutral density filter. A silicon substrate was used to calibrate the Raman shift. An air-tight cell was used for powders, and all sample preparation was done in an argon-filled glovebox. Raman spectra were recorded in the range of 200–3800 cm^{-1} with laser power at 25% and an acquisition time of 30 s and 5 accumulations per run. The reference spectra of Li_2O_2, LiOH, KO_2, LiTFSI and LiI are available in the ESI,† Fig. S6.

Scanning electron microscopy was carried out on a Zeiss Ultra 55, Zeiss Supra 55VP, and a Zeiss Merlin microscope (Carl Zeiss, Germany). The samples were sealed in argon and quickly placed in the vacuum chamber to minimize exposure to ambient atmosphere (maximum 5 seconds). Imaging was performed at a working voltage of 5 kV.

The XRD of discharged products was performed on a Rigaku Smartlab diffractometer in Bragg–Brentano geometry. A domed air tight XRD cell holder from Panalytical was used to prevent exposing the electrodes to ambient atmosphere. The electrodes were washed once in dry solvent before the XRD measurement.

^{1}H NMR was performed on Bruker AVANCE and Bruker AVANCE III-400 MHz nuclear magnetic resonance (NMR) spectrometers. The liquid part of the sample was placed inside the capillary and closed with a Teflon cap. Next, the capillary was placed inside an NMR tube that contained deuterated DMSO solvent. In such a manner, we avoided direct mixing of the reference and sample solutions, so that we could probe the species in the studied solution in isolation. Solids were analysed by first dissolving them in D_2O solution with a known amount of DMSO (3 mM) for quantification purposes. The resulting solution was directly placed in an NMR tube (no capillary).

The Fourier transform infrared (FT-IR) spectra of the materials were obtained on an FT-IR Tensor II (Bruker) inside an argon-filled glovebox with the H_2O and O_2 levels <1 ppm. The measurements were done with a 2 cm^{-1} resolution in the 4000–500 cm^{-1} spectral range; 1000 scans were averaged. The FT-IR spectra were recorded using a single reflection ATR accessory (Pike Vee-Max II, Pike Technologies) with a KRS-5 prism (Pier optics) at an incident angle of 50 degrees.

Results and discussion

Oxidation of I^- to I_3^- and LiOH formation from adding KO_2 to DME-based solutions with low H_2O : LiI molar ratios (<5)

Having KO_2 in DME solutions with LiI could oxidize I^- to I_3^-, as shown in Fig. 1a. Adding KO_2 into the solution (40 ppm of H_2O) with LiTFSI without LiI led to spontaneous oxygen evolution (confirmed by gas chromatography) and precipitation of a white powder, while the solution remained colorless. This observation can be attributed to the well-known disproportionation reaction $2KO_2 + 2Li^+ \rightarrow Li_2O_2 + 2K^+ + O_2$.[1,2] Interestingly, adding KO_2 to the solutions (40 ppm H_2O – 2 mM) containing a mixture of LiTFSI and LiI (H_2O:LiI 0.01) induced an immediate color change to visibly brownish yellow within a few minutes, in addition to gas evolution and precipitation of a white powder (Fig. 1a). It is worth noting that adding KO_2 into solutions containing LiI and 1000 ppm H_2O (48 mM, H_2O:LiI 0.24) led to intensified color changes (Fig. 1a), while no color change was noted for the solutions containing LiTFSI without LiI. Further increasing the water content to 2000 ppm H_2O (96 mM, H_2O:LiI 0.48) and 3000 ppm H_2O (144 mM, H_2O:LiI 0.67) led to even more intense colors (Fig. 1a). The change from colorless to yellow/brown upon addition of KO_2 to solutions containing LiI can be attributed to the formation of triiodide ($3I^- \rightleftharpoons I_3^- + 2e^-$), which is evidenced by the UV-Vis spectra in Fig. 1b. Two new signals appeared at 293 nm and 364 nm, which are characteristic of I_3^-, upon addition of KO_2 while the pristine solution with LiI (colorless) had only I^- adsorption at 230 nm independent of the H_2O content (Fig. S1, ESI†). The formation of I_3^- during Li_2O_2 synthesis has not been reported in the literature during the discharge of batteries[26,34,38] (electrochemical formation of Li_2O_2) as previous studies have shown that the oxidation of I^- to I_3^- occurs during charging and subsequently I_3^- can facilitate the oxidation kinetics of insulating Li_2O_2 through the chemical reaction $Li_2O_2 + I_3^- \rightarrow 2Li^+ + O_2 + 3I^-$.

The concentrations of triiodide (I_3^-), from oxidation of iodide (I^-) in the decanted liquid phase from Fig. 1a, were estimated based on UV-Vis peak intensities at 293 and 364 nm (calibrated with different concentration of I_3^- in Fig. S2, ESI†) shown in Fig. 2 and iodometric titration (Table S1, ESI†). With 40 ppm of

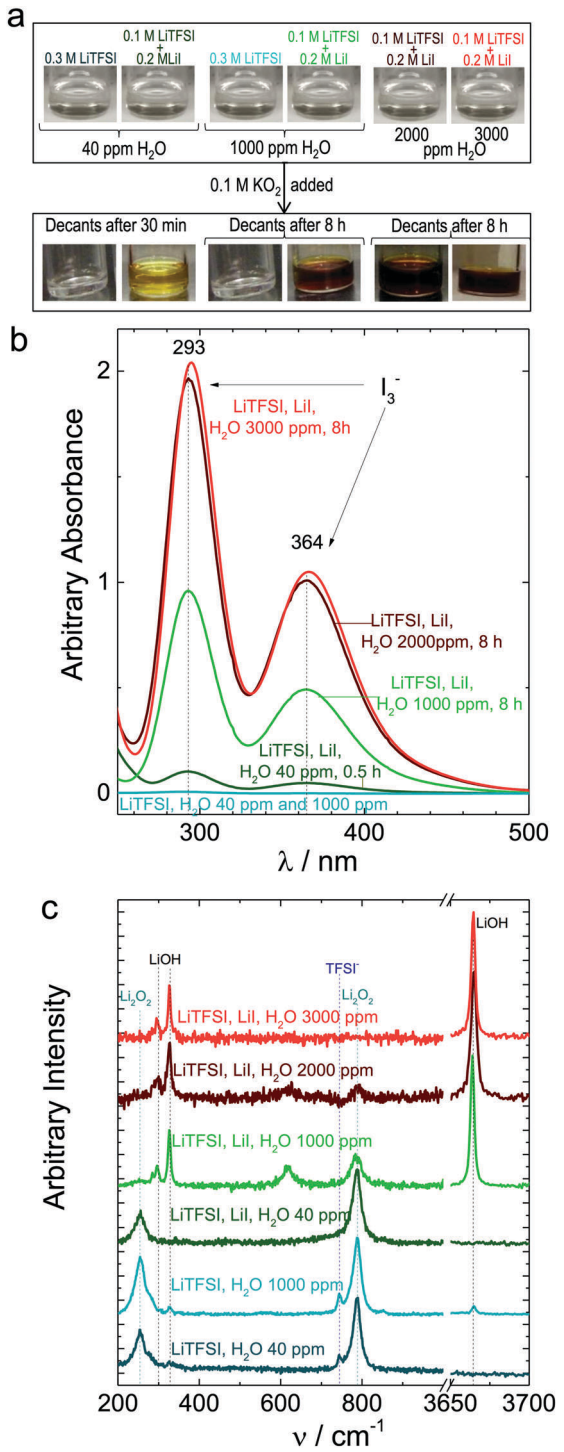

Fig. 1 (a) Changes of DME-based solutions with LiTFSI and LiI before (top) and after (bottom) addition of 0.1 M KO_2, where the concentration of Li^+ was kept constant (0.3 M) and the experiments were performed in argon atmosphere. The bottom images are taken after separation of the solid and liquid phase. (b) The corresponding UV-Vis spectra of the liquid phase obtained after KO_2 addition: blue curves for electrolytes without LiI, dark green for H_2O:LiI 0.01, bright green for H_2O:LiI 0.24, dark red for H_2O:LiI 0.48, and bright red for H_2O:LiI 0.67. (c) The Raman spectra of the corresponding solid phase obtained after KO_2 addition. Raman spectra were recorded in the range of 200–3800 cm^{-1} with a laser power of 25% and an acquisition time of 30 s and 5 accumulations. The reference spectra of Li_2O_2, LiOH, KO_2, LiTFSI and LiI are available in the ESI,† Fig. S6.

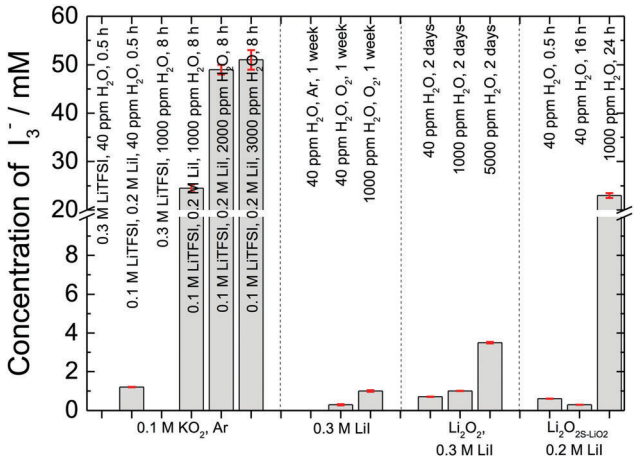

Fig. 2 The concentrations of I_3^- estimated from UV-Vis spectroscopy based on three sets of experiments (left from Fig. 1 and center and right from Fig. 3). The error bars are indicated in red. The I_3^- concentration measurement errors came mostly from the solution preparation by pipetting, which had 1% volume error (based on the pipette specifications) when operated with volumes above 50% of its maximum value. Thus, it was dependent on the number of dilutions and was estimated to be 1%, 2% and 3% for dilution of 1, 2 and 3 times, respectively. The accuracy of the UV-Vis experiment was confirmed by iodometric titration which gave almost identical I_3^- concentrations (Fig. S4 and Table S1, ESI†).

H_2O (2 mM), the I_3^- concentrations detected were low, which was independent of initial LiI concentrations added (1.0 to 1.3 mM), as shown in Fig. S3a (ESI†). In addition, the I_3^- concentration reduced with increasing reaction time, dropping from 1.2 mM after 0.5 hour to 0.01 mM after 24 hours, as shown in Fig. S3b (ESI†). The slow decay of I_3^- concentration with time can be related to the oxidation of Li_2O_2 obtained from the disproportionation reaction, which is accompanied by reduction of I_3^- to I^- ($Li_2O_2 + I_3^- \rightarrow 2Li^+ + O_2 + 3I^-$). Increasing H_2O from 40 to 1000 ppm (48 mM), the I_3^- concentration was increased to ~25 mM, as shown in Fig. 2. The formation of I_3^- occurred rapidly, reaching 25 mM after 4 hours, and then decreased by a minute amount over a long time (to 24 mM after 24 hours), as shown in Fig. S4 (ESI†). The formation of I_3^- can be explained by the following mechanism with reactions (4)–(6) below, which would yield half I_3^- relative to H_2O added in a molar ratio as observed experimentally. This mechanism is supported by the fact that increasing water levels to 2000 ppm (96 mM) doubled the I_3^- concentration to 49 mM. Further increasing to 3000 ppm (142 mM) did not increase the I_3^- concentration, as shown by both UV-Vis and iodometric titration after 8 hours in Fig. 2. Therefore, the concentrations of I_3^- detected (50 mM) were no longer limited by H_2O available in the electrolyte when above 2000 ppm (96 mM). Instead they were limited by the amount of KO_2 added (0.1 M) in the experiments, where the maximum amount of H_2O_2 (50 mM) available to oxidize I^- is limited by the maximum amount of Li_2O_2 potentially formed (50 mM) from the disproportionation of 0.1 M KO_2.

$$2LiO_2 \rightarrow Li_2O_2 + O_2 \quad (4)$$

$$Li_2O_2 + 2H_2O \rightarrow H_2O_2 + 2LiOH \quad (5)$$

$$H_2O_2 + 3I^- + 2Li^+ \rightarrow 2LiOH + I_3^- \quad (6)$$

This mechanism is supported by the ^{1}H NMR spectra of the liquid phase (Fig. S5, ESI†), which revealed that H_2O was consumed completely for samples containing LiI and H_2O levels up to 2000 ppm (96 mM) but not for 3000 ppm (142 mM). The sample with 1000 ppm H_2O and LiTFSI (without LiI) showed a strong signal from H_2O, indicating that H_2O remains intact during the disproportionation reaction without LiI. Moreover, the ^{1}H NMR spectra of the liquid phase revealed a lack of soluble decomposition products of DME (Fig. S5, ESI†).

The Raman spectroscopy of the collected precipitates, obtained from adding KO_2 to DME solution containing LiTFSI and LiI provided further support to the mechanism (reactions (4)–(6)). Li_2O_2 was the major phase for the low H_2O content of 40 ppm, as evidenced by the appearance of peaks at 254 and 787 cm^{-1} (Fig. 1c), in agreement with the Raman spectra of commercial Li_2O_2 powder (Fig. S6, ESI†). Increasing the H_2O content from 40 to 1000 ppm for a mixture with LiTFSI only, led to the formation of a small amount of LiOH, with the majority of the precipitate being identified as Li_2O_2, which is in accordance with previous reports.[46] In contrast, the presence of LiI (and 1000 ppm H_2O) produced a mixture of LiOH and Li_2O_2, with high content of the former. Increasing the H_2O content from 1000 ppm to 2000 ppm in the presence of LiI further produced more LiOH and less Li_2O_2. And finally, with 3000 ppm of H_2O, a pure LiOH phase was obtained. Therefore, disproportionation of KO_2 in the solution with both high H_2O content and LiI led to the formation of LiOH, which is consistent with previous studies.[26,35] In this study, we propose that the formation of LiOH can be attributed to deprotonation of H_2O and, by a much smaller extent, DME in the presence of strong oxidants such as Li_2O_2 and LiO_2, which will be discussed and examined below. The deprotonation/degradation of DME is supported by the ^{1}H NMR spectra of the solid phase (Fig. S7, ESI†), which revealed a small amount of $HCOO^-$ and CH_3COO^- corresponding to about 0.1–0.2 mM of reacted DME. Although the decomposition of DME is not significant, cycling can lead to the accumulation of by-products and can shorten the cycle life of Li–O_2 batteries.

It is worth noting that the greater the I_3^- concentration in the liquid phase from the mixture in Fig. 1a, the greater the amount of LiOH relative to Li_2O_2 (Fig. 1c). It is proposed that I^- can be oxidized to I_3^- by peroxy-like species such as hydrogen peroxide[43] or the hydroperoxyl anion (HO_2^-).[47] For example, the reaction may proceed in two steps: $H_2O_2 + I^- \rightarrow IO^- + H_2O$ and $IO^- + 2I^- + H_2O \rightarrow I_3^- + 2OH^-$.[43,47] There are a number of reactants that can generate H_2O_2: KO_2, O_2, O_2^-, HO_2, LiO_2 and Li_2O_2, which can form upon adding KO_2 into LiI-containing DME solutions with H_2O. We conducted additional experiments to understand what reactions are most likely to be responsible for the observed oxidation of I^- to I_3^- and the associated LiOH formation found in Fig. 1.

Minimal influence of molecular oxygen on the oxidation from I^- to I_3^-

We first examine the effect of molecular oxygen on the degree of oxidation from I^- to I_3^-, which may occur by direct oxidation of I^- in the solution or by H_2O_2 formed from self-oxidation of DME by molecular oxygen ($RH + O_2 \rightarrow R^* + HOO^*$ and $RH + HOO^* \rightarrow R^* + H_2O_2$).[48–50] The UV-Vis spectra of 0.3 M LiI solution in DME (either 40 ppm or 1000 ppm of H_2O) under argon and oxygen are compared in Fig. 3a. Under argon, the solution remained colorless after 1 week, having only signals from I^- (below 270 nm) with no trace of triiodide. In contrast, under oxygen the solution became yellowish, and two triiodide signals appeared on the UV-Vis spectra, but the triiodide concentration was low (0.31 mM after 1 week, Fig. 2). We can rule out the direct oxidation of iodide by molecular oxygen as when replacing DME with DMSO as the solvent, we found no triiodide formed in the presence of O_2 (Fig. S8, ESI†). In addition, we found that light can promote the oxidation from I^- to I_3^-, as indicated by an observed doubling of the concentration of I_3^- relative to a solution aged in the dark as shown in Fig. S8 (ESI†), which might be attributed to the enhanced kinetics of self-oxidation of DME to form more H_2O_2.[48–50] Moreover, adding extra H_2O to the solution (1000 ppm) can further accelerate DME self-oxidation[48–50] as the amount of I_3^- detected was three times higher as compared to the 40 ppm solution. Nevertheless the amount still remained low after 1 week (0.95 mM). Therefore, such small concentrations of I_3^- detected and slow kinetics (1 week to obtain 0.95 mM I_3^-, representing 1% conversion of iodide) cannot account for the significant amount of I^- oxidation found in the presence of KO_2 and Li^+, where a strong color change was observed in the first few minutes and 25–50 mM of I_3^- (37.5–75.0% conversion of iodide) was detected after 8 hours.

We would like to note that the oxygen used in this study was in its ground state (triplet). During the disproportionation reaction, singlet oxygen can be produced that can easily react with H_2O or DME to form H_2O_2 according to recent studies by Mahne *et al.*[51] However, the amount of singlet oxygen formation during the disproportionation reaction of LiO_2 is very low relative to the total amount of evolved oxygen, thus, it cannot account for the equimolar formation of I_3^-. This is supported by the results of the disproportionation experiment in the presence of only LiTFSI salt and 1000 ppm of H_2O where H_2O_2 at a concentration <0.5 mM was detected with Quantofix strips (sigma Aldrich) in the liquid phase. The concentration was further confirmed by adding LiI to the decanted liquid phase and quantifying the amount of formed I_3^- by UV-Vis (0.43 mM). Therefore, the role of molecular oxygen in I_3^- formation is found to be minor in the time scale of a day.

Minimal role of superoxide O_2^- and KO_2 in the formation of LiOH and oxidation from I^- to I_3^-

Here we examine the role of superoxide ions (O_2^-) and KO_2 in forming LiOH *via* deprotonation of DME[48]/H_2O[46] and creation of hydroperoxyl ions HO_2^-,[46,48,49,52] which can oxidize I^- to I_3^- (detailed mechanism in ESI†). 300 mM KI was used to replace LiI; adding 100 mM KO_2 to the solution with 40 or 1000 ppm did not lead to disproportionation, precipitation, or gas evolution. The UV-Vis spectra of the solutions exhibited a broad signal between 200–400 nm (Fig. 3b), which can be attributed to O_2^-,[53] and weak

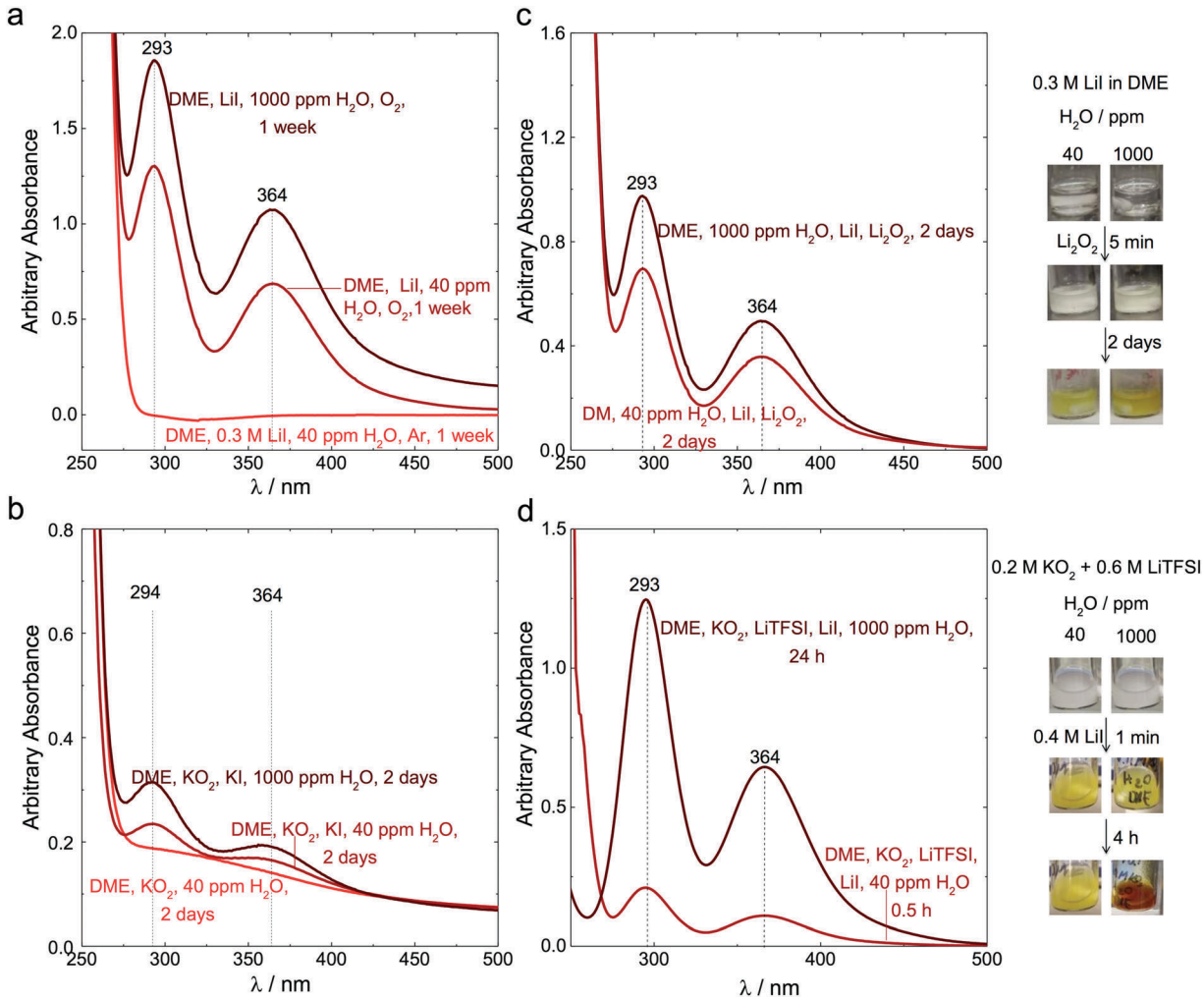

Fig. 3 (a) The influence of O_2 and H_2O on the stability of I^- in DME solution. UV-Vis spectra of 0.3 M LiI solutions in DME with either 40 ppm H_2O (H_2O:LiI 0.007) or 1000 ppm H_2O (H_2O:LiI 0.16). The spectra are taken after 1 week of storage in defined conditions. (b) UV-Vis spectra of DME with either 40 ppm H_2O (H_2O:LiI 0.007) or 1000 ppm H_2O (H_2O:LiI 0.16) mixtures containing 0.1 M KO_2 and 0.3 M KI after 2 days. The I_3^- concentration from absorption values at 293 nm and 364 nm was estimated after subtraction of the reference DME + KO_2 spectra to avoid contribution from O_2^- absorption. (c) The UV-Vis spectra of 0.3 M LiI mixed with commercial Li_2O_2 powder (0.1 g) in DME with 40 ppm (H_2O:LiI 0.007) or 1000 ppm of H_2O (H_2O:LiI 0.16) after 2 days. The inset on the top right shows optical photographs of the mixture after 5 minutes and 2 days. (d) UV-Vis spectra of 0.2 M LiI + 0.3 M LiTFSI solution in DME with either 40 ppm H_2O (H_2O:LiI 0.01) after 0.5 hour or 1000 ppm of H_2O (H_2O:LiI 0.24) after 24 hours. 0.2 M KO_2 was added first to a 0.6 M LiTFSI solution leading to the formation of Li_2O_2–S-LiO_2, and after 20 minutes, 0.4 M LiI solution was added. The inset on the bottom right shows optical micrographs of the mixture after 1 minute and 4 hours.

signals of I_3^-. Although increasing H_2O from 40 to 1000 ppm increased the intensity of I_3^- signals, the concentrations were found to be below 0.01 mM and the solution remained visibly clear after addition of KO_2 for 2 days. We further increased the concentration of soluble KO_2 in the solution by replacing DME with DMSO[41] (Fig. S9, ESI†). Nevertheless, the concentration of I_3^- was lower than 0.01 mM (similar to that found in DME). Therefore, we conclude from these observations that O_2^- and KO_2 play a negligible role in deprotonating DME or H_2O to produce the observed LiOH and detection of 25–50 mM for I_3^- found in Fig. 1.

Minor role of commercial Li_2O_2 powder on the formation of LiOH and oxidation from I^- to I_3^-

Commercial Li_2O_2 powder (Alfa Aesar, 500–1000 nm particle size in Fig. S10a (ESI†), 100 mg) was added to solutions containing 0.3 M LiI and 40 or 1000 ppm H_2O in DME. No color change was observed after 5 minutes while both solutions became yellowish after 2 days, as shown in Fig. 3c. The UV-Vis spectra (Fig. 3c) of solutions with 40 and 1000 ppm H_2O revealed I_3^- at concentrations of 0.71 and 1.0 mM after 2 days, respectively. I_3^- concentrations increased further to 3.5 mM when a solution with 5000 pm H_2O was used (Fig. S11, ESI†). The oxidation kinetics for this case (no color changes after minutes and 1.0 mM, representing 1% oxidation, after 2 days) is much slower than that observed when adding KO_2 to Li^+-containing DME solution (strong color changes after few minutes and 25–50 mM, representing 37.5–75.0% oxidation after 8 hours). The slow reaction process is further supported by SEM images, where no change in Li_2O_2 morphology was observed after 2 days of reaction (Fig. S10a, ESI†). Therefore, commercial Li_2O_2 particles

were found to play a minor role in deprotonating DME and H_2O and the observed oxidation in Fig. 1. However, commercial Li_2O_2 powder still led to a notably higher concentration of I_3^- (>1 mM after 2 days) when compared with molecular oxygen (0.95 mM after 1 week) and O_2^- and KO_2 (<0.01 mM after 2 days), as shown in Fig. 2. The slow kinetics of I^- oxidation and LiOH formation in the presence of commercial Li_2O_2 shown in Fig. 3c might be attributed to the possibility that Li_2O_2 particle surfaces were covered by LiOH, as this commercial Li_2O_2 was ~86% phase with ~13% LiOH.[42] In the following section, we performed comparable experiments to Fig. 3c using Li_2O_2 formed from disproportionation. As our previous X-ray absorption measurements[10] have shown that Li_2O_2 formed from disproportionation at high discharge voltages in Li–O_2 cells has more oxygen-rich containing LiO_2-like species on the surface, we denote such Li_2O_2 as $Li_2O_{2S\text{-}LiO_2}$.

Significant role of $Li_2O_{2S\text{-}LiO_2}$ produced by disproportionation in the formation of LiOH and oxidation from I^- to I_3^-

We first produced $Li_2O_{2S\text{-}LiO_2}$ (200–1000 nm, Fig. S10b, ESI†) from disproportionation by mixing 0.2 M KO_2 and 0.6 M LiTFSI in a DME solution containing either 40 or 1000 ppm of H_2O for 20 min. A 0.4 M LiI solution was added subsequently to the solution, so that the final concentration of the species was 0.3 M LiTFSI and 0.2 M LiI. A few seconds after adding LiI, the color changed from clear to yellowish in both solutions. UV-Vis measurements revealed small concentrations of I_3^- (0.62 mM) for the solution with 40 ppm H_2O after 30 minutes (Fig. 3d), that faded with time (0.31 mM after 16 hours). Remarkably, the color of the solution with 1000 ppm of H_2O became brownish after 4 hours, indicating an increase in I_3^- concentration with time. Indeed, within the first 24 hours the I_3^- concentration increased, reaching a maximum value of 23 mM, as shown in Fig. S12 (ESI†) and Fig. 2. After 24 hours, a small decrease in I_3^- concentration was observed. This trend is very similar to the one found in Fig. S4 (ESI†), where KO_2 was added directly to the solution containing LiI. However, the kinetics of I_3^- formation is slower as the maximum concentration is reached after 24 hours in Fig. S12 (ESI†) as compared with 8 hours in Fig. S4 (ESI†). The decomposition of Li_2O_2 and formation of LiOH is further supported by SEM images, where after reaction we observed transformation of small rough Li_2O_2 particles into big particles (few μm in size) with smooth facades (Fig. S10b, ESI†).

The faster kinetics and greater extent of oxidation of I^- to I_3^- found for $Li_2O_{2S\text{-}LiO_2}$ produced by disproportionation than for commercial Li_2O_2 (Fig. 2) can be attributed to the possibilities that (1) commercial Li_2O_2 particle surfaces might be passivated by LiOH and (2) $Li_2O_{2S\text{-}LiO_2}$ prepared from disproportionation can have LiO_2 on the surface,[10] which could deprotonate H_2O more readily. On the other hand, the faster kinetics of I_3^- formation when KO_2 is added directly to the solution containing LiI, can be related to either the presence of soluble LiO_2 or small aggregates/clusters of Li_2O_2[54,55] during the O_2^- disproportionation reaction, which can be more reactive[56] towards the deprotonation of H_2O/DME than $Li_2O_{2S\text{-}LiO_2}$ particles (200–1000 nm), which were produced by disproportionation in advance, Fig. 3. Considering that soluble LiO_2 most likely disproportionates faster (second order[55] $k \approx 20\ M^{-1}\ s^{-1}$, first order[41] $k \approx 5\ s^{-1}$) than deprotonating H_2O ($k \approx 10^{-3}\ M^{-1}\ s^{-1}$ in acetonitrile and dimethylformamide),[52] reaction products of LiO_2 disproportionation may contribute to deprotonation of H_2O to a greater extent than soluble LiO_2. Therefore, it is proposed that the main oxidants responsible for the deprotonation of H_2O to form LiOH and the oxidation of I^- to I_3^- are small aggregates/clusters of LiO_2-like and Li_2O_2-like species formed during disproportionation. Finally, the following mechanism is proposed: Li_2O_2 can react with H_2O to produce LiOH and H_2O_2 ($Li_2O_2 + 2H_2O \leftrightarrow 2LiOH + H_2O_2$),[46] the latter H_2O_2 can then oxidize I^- to I_3^-[43] leading to high concentrations of I_3^- which strictly depend on the amount of Li_2O_2 and H_2O available. The consumption of H_2O was indeed observed from the ^1H NMR spectra of the solution before and after oxidation of I^- (Fig. S5, ESI†), while the conversion of Li_2O_2 to LiOH was confirmed by Raman spectroscopy, Fig. 1c. Moreover, LiO_2/Li_2O_2 or singlet oxygen can deprotonate DME[26,51,57] to form HOO^- and H_2O_2, which can oxidize I^- to I_3^- ($Li_2O_2 + CH_3O - R_1 \leftrightarrow CH_3OLi + R_2 + HOO^-Li^+$), as suggested by the ^1H NMR spectra of the solid phase, Fig. S7 (ESI†). Nevertheless, the concentration of I_3^- from this process is very small, <1 mM, as judged by the amount of decomposition products. It is worth noting that the decomposition of DME is independent of the presence of LiI as similar by-products were found in the mixture with only LiTFSI salt and previous studies of Li–O_2 electrochemistry in DME.[48,58] This point is in contrast to that of Kwak *et al.*,[26] who suggested that LiOH formation is mostly due to decomposition of the TEGDME electrolyte when electrolytes with high concentrations of LiI are used. In our case, the LiOH and I_3^- formation was independent of the LiI concentration (Fig. S3b, ESI†). This difference might be either related to the TEGDME solvent (DME was used here) or the uncontrolled amount of water in LiI (Kwak *et al.*[26] did not provide H_2O content in the electrolyte, while in this study, pure DME had H_2O of 6 ppm and the electrolyte had 40 ppm of H_2O after addition of high-purity salts). Deprotonation of both H_2O and DME could explain the I_3^- concentration of 1.2 mM for the electrolyte containing only 40 ppm (2 mM) of water as from 2 mM of H_2O only 1 mM I_3^- can be produced, indicating that the remaining 0.2 mM comes from DME decomposition.

Lastly, our results indicate that in a DME-based system, triiodide has sluggish kinetics towards Li_2O_2 oxidation from Fig. S3, S4 and S12 (ESI†), where a decrease in I_3^- concentration due to reaction with Li_2O_2 takes hours and even days, which is in agreement with Burke *et al.*[38] More systematic studies are needed to evaluate the effectiveness of the iodide in different electrolytes for Li_2O_2 oxidation upon discharge and charge of Li–O_2 batteries.

The formation of LiOH facilitated by LiI at low H_2O : LiI ratios (up to 5)

The presence of 1000 ppm H_2O without LiI is not sufficient to produce LiOH as adding KO_2 into LiTFSI containing solutions

generates Li_2O_2 only (blue spectra in Fig. 1c), which is in agreement with the literature.[46] The greater the amount of I_3^- detected in Fig. 1, the greater the amount of LiOH relative to Li_2O_2. This correlation (Fig. 2) suggests that the formation of LiOH in these experiments needs to be facilitated by LiI. Below, we discuss two processes by which LiI can promote the deprotonation of H_2O and facilitate LiOH formation. Considering that the free energy change for the reaction $Li_2O_2 + 2H_2O \rightleftharpoons H_2O_2 + 2LiOH$ ($\Delta G^\circ = 41$ kJ mol^{-1})[59] is close to zero, where the equilibrium amounts of H_2O_2 and LiOH produced are small. First, the consumption of H_2O_2 by LiI (*via* $H_2O_2 + I^- \rightarrow IO^- + H_2O$ and $IO^- + 2I^- + H_2O \rightarrow I_3^- + 2OH^-$) can strongly drive the reaction equilibrium to the right, consuming available Li_2O_2 and generating I_3^- and LiOH. Second, the presence of LiI can increase the activity of H_2O in DME, which makes it easier to deprotonate H_2O. Kwabi *et al.*[46] have shown that the pK_a of H_2O in different solvents can influence the Li–O_2 product chemistry: H_2O in pure DME has a high pK_a, resulting in low H_2O reactivity and thus no LiOH formation in the presence of H_2O, while H_2O in acetonitrile (MeCN) has a lower pK_a, resulting in LiOH formation, in addition to Li_2O_2, during discharge of Li–O_2 cells.[46] Similarly, Che *et al.*[52] reported that the pK_a of water was modified by the surrounding solvent, which in turn affects the mechanism of superoxide disproportionation. Adding LiI to DME can lower the H_2O pK_a in DME due to the strong interactions between iodide ions and H_2O expected from hydrogen/halogen bonding.[60,61] This hypothesis is supported by the following ^{1}H NMR and FT-IR experiments discussed below.

The H_2O peak in the ^{1}H NMR spectra (Fig. 4a) was found to shift from 2.4 ppm to 4.3 ppm upon the addition of LiI salt to DME with 1000 ppm H_2O (H_2O:LiI 0.16) while the addition of LiTFSI caused a shift from 2.4 to 3.4 ppm, as shown in Fig. 4a. Following the trend established by Forsyth and Macfarlane *et al.*,[62] where the higher the shift of ^{1}H NMR, the more acidic the protons are, LiI addition in DME increased the acidity of H_2O. Further support comes from the FT-IR measurements shown in Fig. 4b. The O–H stretching band ($\sim$3600 cm^{-1}) of H_2O from DME-based solutions with 1000 ppm (H_2O:LiI 0.16) and 5000 ppm (H_2O:LiI 0.80) was shifted to lower wavelengths ($\sim$3400 cm^{-1}) and was shown to have higher intensities upon addition of LiI. These changes can be attributed to the formation of hydrogen/halogen bonds that alter the strength of the O–H bond resulting in weaker O–H bonding and stronger acidity of H_2O.[63–65]

The formation of LiOH·H_2O at high H_2O : LiI ratios (greater than 5)

We further conducted similar disproportionation experiments to those discussed above using electrolytes with exceptionally high water levels,[32,35] and more precisely high H_2O : LiI ratios (>5). Lowering the acidity of H_2O (increasing deprotonation energy or pK_a) was found to promote reaction products like LiOH·H_2O instead of LiOH from H_2O and Li_2O_2. The acidity of H_2O was decreased by increasing the H_2O : LiI ratio from 0.25 to 12, which was accompanied with increasing H_2O : DME ratios from 0.0078 to 0.86 in the electrolyte, as indicated by a

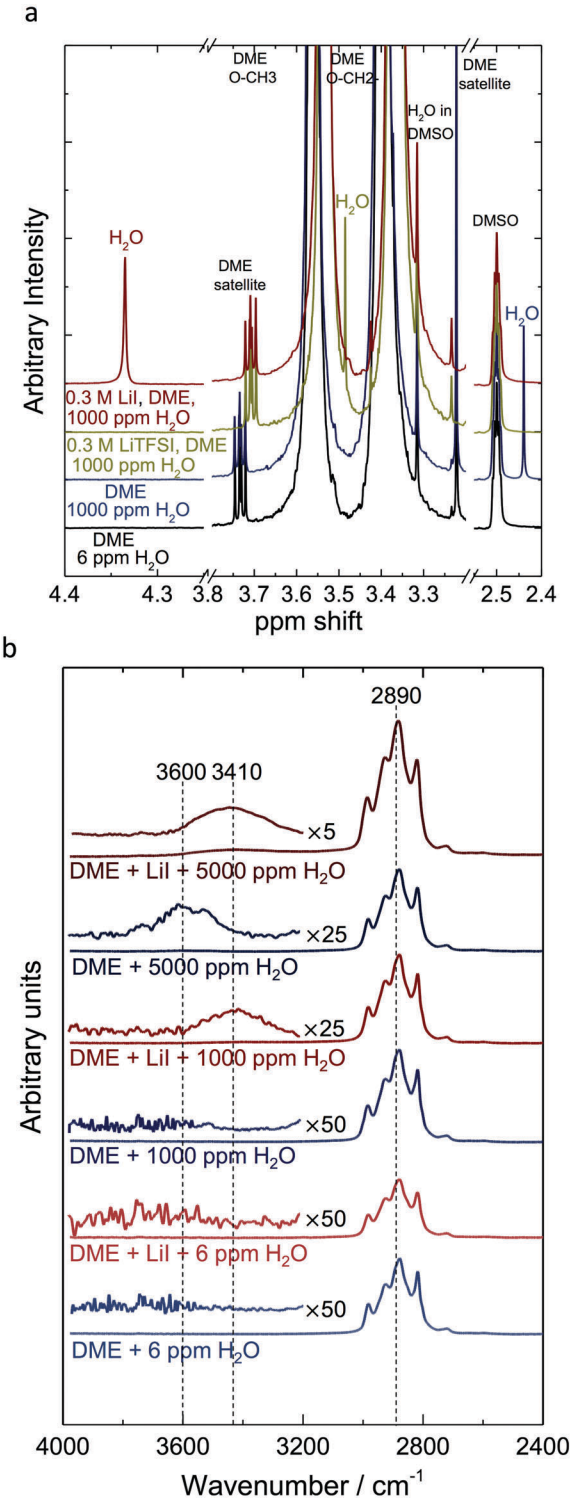

Fig. 4 (a) The ^{1}H NMR spectra of DME solutions with 6 ppm of H_2O – black curve, 1000 ppm of H_2O – blue curve, 0.3 M LiTFSI and 1000 ppm of H_2O – green curve, or 0.3 M LiI and 1000 ppm of H_2O (H_2O:LiI 0.16) – red curve. The NMR experiment was performed with an internal capillary that allows for separation of the studied sample from the deuterated solvent. The ^{1}H NMR signal of pure H_2O at T = 298 K is 4.8 ppm. (b) The FT-IR spectra of pure DME and 0.3 M LiI solution in DME with different H_2O content: 6 ppm (H_2O:LiI 0.003), 1000 ppm (H_2O:LiI 0.16), 5000 ppm (H_2O:LiI 0.80).

systematic negative shift in the H_2O ^1H NMR signal (from 4.4 to 3.7 ppm) in Fig. 5a. In contrast, increasing H_2O : DME ratios without LiI in the electrolyte increased H_2O acidity as shown by a systematic positive shift in the H_2O ^1H NMR signal from 2.5 ppm for H_2O:DME of 0.0078 to 3.8 ppm for H_2O:DME of 0.86, as shown in Fig. 5b. These changes in H_2O acidity can be attributed to competing solvation of H_2O among H_2O, DME[46] and LiI[66] with increasing H_2O : DME and H_2O : LiI ratios. As discussed previously, the large increase in the H_2O acidity in the presence of LiI can be attributed to strong interactions between I^- and protons in H_2O solvated largely by DME at low H_2O : DME ratios. The difference in the H_2O acidity between electrolyte solutions with and without LiI decreased with increasing H_2O : DME and corresponding H_2O : LiI ratios, and became diminished at a H_2O : DME ratio of 0.86, as shown in Fig. 5c. The comparable H_2O acidity with and without LiI at high H_2O : LiI and H_2O : DME ratios can be attributed to weaker interactions between I^- and protons of H_2O due to greater solvation of H_2O in H_2O than DME,[66] and fewer I^- interacting with H_2O than solutions with low H_2O : LiI ratios. These observations are further supported by FT-IR measurements (Fig. S13, ESI†), where for H_2O : LiI ratios lower than 5 the O–H stretching band was blue shifted (centred at 3394 cm^{-1}) as compared to solutions without LiI (centred at 3540 cm^{-1}), indicating greater acidity. Additionally, we observed the appearance of the H_2O bending band at 1647 cm^{-1} (Fig. S14, ESI†) for H_2O : LiI ratios higher than 5, suggesting increased solvation of H_2O by H_2O. Therefore, the H_2O acidity in these H_2O:LiI:DME solutions can be tuned by two competing effects of greater H_2O solvation than DME to increase the H_2O acidity and lower interaction between I^- and protons to reduce H_2O acidity with increasing H_2O : DME ratio. Lastly, our solutions with H_2O : LiI ratios of 12 and 24 without LiTFSI were found to have comparable H_2O acidity to that used previously[32] (H_2O:LiI of 134, H_2O:DME of 0.57 and 0.5 M LiTFSI) in Fig. 5c. Adding LiTFSI into the solution with H_2O : LiI ratios of 12 and 24 increased the water acidity, which was higher than that for H_2O:LiI of 134.

With H_2O : LiI ratios lower than 2, the amount of I_3^- detected from the disproportionation reaction by mixing 0.3 M LiI solution with 0.1 M KO_2 for 24 hours was close to ~50 mM in Fig. 5c, which is the maximum estimated from 0.1 M KO_2 based on the proposed mechanism (reactions (4)–(6)). Increasing H_2O : LiI ratios from 2 to 5 sharply reduced the amount of I_3^-, which became negligible for H_2O : LiI ratios of 12 and 24. Such changes were visible as the suspension changed from dark brown for H_2O : LiI molar ratios lower than 2 to light brown, yellow or colorless for H_2O : LiI molar ratios of 5, 12 and 24 after a few minutes, respectively. Lower I_3^- found for high H_2O : LiI ratios can be attributed to lowered acidity of H_2O, which reduces the reactivity of H_2O towards Li_2O_2 or LiO_2 to produce H_2O_2, and thus decreases the amount of I_3^- oxidized from I^- by H_2O_2 (reactions (5) and (6)).

Raman spectroscopy showed that the solid reaction products obtained from low H_2O acidity at high H_2O : LiI molar ratios of 24 (having 0.3 M LiI and H_2O:DME of 0.86 and 0.5 M LiTFSI) and 134 (having 0.03 M LiI and H_2O:DME of 0.58 and 0.5 M

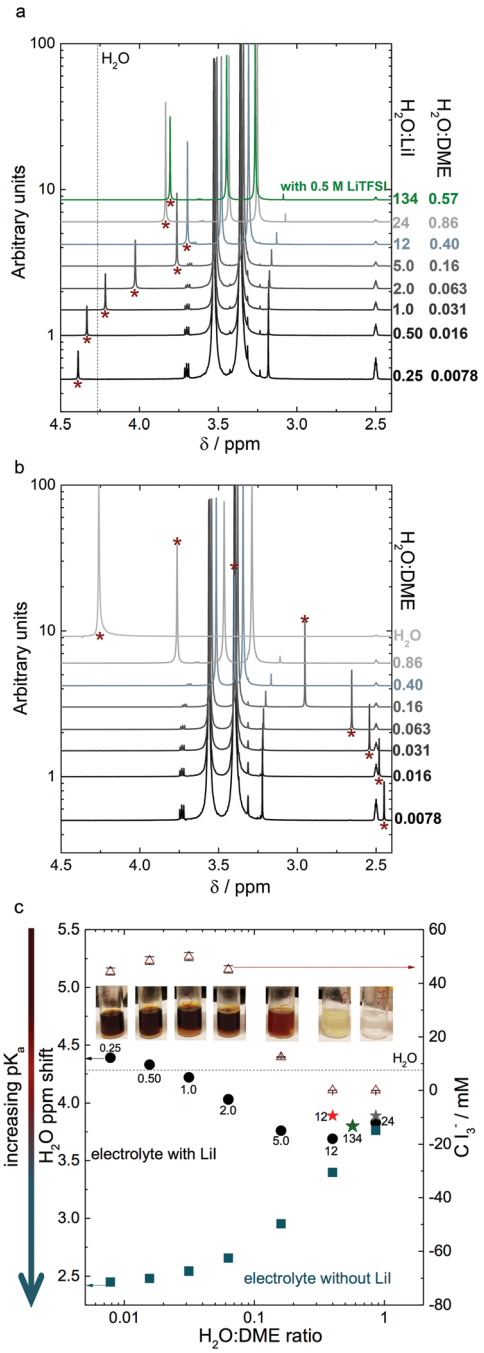

Fig. 5 (a) ^1H NMR spectra of H_2O:DME mixtures; the molar ratios of H_2O : DME are indicated on the right. The water peaks are assigned with a star sign. (b) ^1H NMR spectra of 0.3 M LiI in H_2O:DME mixtures, with the molar ratios of H_2O : LiI and H_2O : DME indicated on the right. The dashed line represents the H_2O signal shift of pure H_2O. (c) The shift of the H_2O signal (left axis) as a function of H_2O : DME ratio for the H_2O : DME mixture with LiI (black, the numbers near the data points indicate the H_2O : LiI molar ratio) and without LiI (navy). The stars indicate the H_2O ppm shift for electrolytes with 0.5 M LiTFSI, red and gray stars are for solutions with 0.3 M LiI and the red star is for a solution with 0.03 M LiI (same composition as in ref. 32). The arrow indicates the relation between pK_a and H_2O signal shift. The right axis shows the concentration of the I_3^- formed during the LiO_2 disproportionation reaction (0.3 M LiI + 0.1 M KO_2 for 24 h), where the optical images of suspensions after 24 hours are shown. The calculation details of the error bars can be found in the Experimental.

LiTFSI – composition identical to ref. 32) for 1 hour consisted of Li_2O_2, $LiOOH{\cdot}H_2O$ and $LiOH{\cdot}H_2O$. $LiOH{\cdot}H_2O$ was the major phase for H_2O:LiI of 24 while Li_2O_2 was the major phase from solution for H_2O:LiI of 134. Such a difference could result from the lower acidity of H_2O (3.8 ppm) for the H_2O : LiI ratio of 134 and 0.5 M LiTFSI than that (3.9 ppm) for the solution with the H_2O : LiI ratio of 24 and 0.5 M LiTFSI as indicated by the ^{1}H NMR spectra in Fig. S15 (ESI†) and shown in Fig. 5c. In addition, extending the reaction time to 48 hours for the H_2O : LiI molar ratio of 134 yielded much less Li_2O_2 and significantly more $LiOH{\cdot}H_2O$ while the Raman peak intensities from $LiOOH{\cdot}H_2O$ did not change significantly relative to that obtained from 1 hour. Reduction of Li_2O_2 with reaction time can be explained by the reactivity between Li_2O_2 with H_2O to form $LiOOH{\cdot}H_2O$, which decomposes to $LiOH{\cdot}H_2O$ according to reactions (7) and (8). The formation of $LiOOH{\cdot}H_2O$ (reaction (7)) instead of H_2O_2 (reaction (5)) can be attributed to lower H_2O acidity and reactivity with Li_2O_2 at higher H_2O : LiI molar ratios. The formation of $LiOOH{\cdot}H_2O$ and $LiOH{\cdot}H_2O$ does not generate H_2O_2, which is consistent with the absence of oxidation of I^- to I_3^-. The disproportionation reaction mechanisms for different H_2O : LiI ratios are summarized in Fig. 7a.

$$Li_2O_2 + 3H_2O \rightarrow LiOOH{\cdot}H_2O + LiOH{\cdot}H_2O \quad (7)$$

$$2LiOOH{\cdot}H_2O \rightarrow 2LiOH{\cdot}H_2O + O_2 \quad (8)$$

We note that the detection of $LiOOH{\cdot}H_2O$ and $LiOH{\cdot}H_2O$ in the reaction product solids was dependent on experimental conditions. We found that the addition of LiTFSI to the H_2O:LiI:DME solutions promotes the formation of $LiOOH{\cdot}H_2O$ relative to Li_2O_2. Conducting the disproportionation reaction (0.3 M LiI + 0.1 M KO_2 in Fig. 6) without LiTFSI yielded no detectable $LiOOH{\cdot}H_2O$ but Li_2O_2 as the major phase with a small amount of $LiOH{\cdot}H_2O$ after 1 hour, and $LiOH{\cdot}H_2O$ as the only phase after 24 hours, as shown in Fig. 6. The formation of $LiOOH{\cdot}H_2O$ instead of Li_2O_2 with the addition of LiTFSI to the suspension with H_2O:LiI of 24 (Fig. 6) is consistent with the absence of I_3^-, and $LiOOH{\cdot}H_2O$ converted quickly to $LiOH{\cdot}H_2O$ by disproportionation within 1 hour. This observation can be attributed to greater acidity of H_2O, as indicated by positive peak shifts for the H_2O signal (Fig. 5c and Fig. S15, ESI†). Moreover, washing reaction solid products with anhydrous DME led to the formation of LiOH from the disproportionation reaction with H_2O : LiI ratios from 0.25 to 24 without LiTFSI for 24 hours, presumably due to the dehydration of $LiOH{\cdot}H_2O$ at low H_2O : DME ratios during washing with anhydrous DME (Fig. S16, ESI†).

The influence of LiI on the discharge product chemistry in Li–O_2 cells

In our studies of Li–O_2 battery discharge, we will limit our experiments to low H_2O:LiI levels (<1) as results for high water levels, and H_2O : LiI ratios have been reported in the recent studies of Zhu *et al.*[32] CNT electrodes were discharged in Li–O_2 cells with 0.3 M LiTFSI or 0.1 M LiI + 0.2 M LiTFSI under potentiostatic (2.7 and 2.2 V_{Li}) and galvanostatic (12.5 mA g^{-1}_{CNT}) conditions to capacities of $\sim$4000 mA h g^{-1} (Fig. 8). Adding 1000 ppm H_2O (H_2O:LiI 0.48) greatly increased the currents found

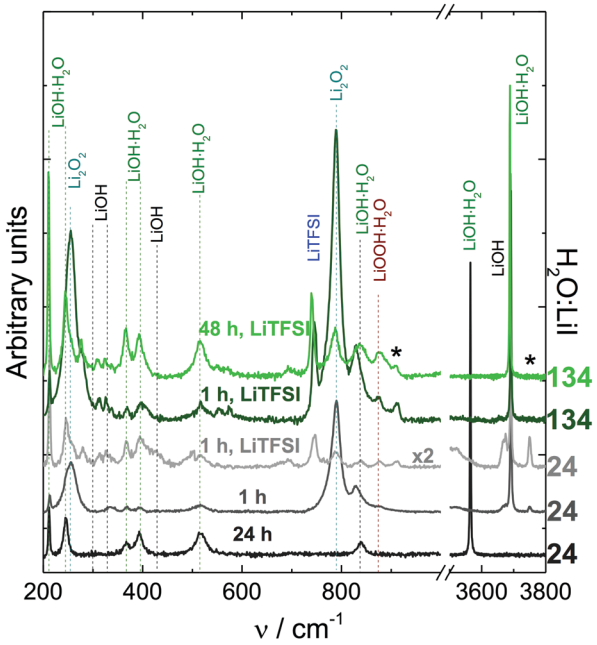

Fig. 6 Raman spectra of unwashed powders obtained from the disproportionation reaction (0.3 M LiI + 0.1 M KO_2): H_2O : LiI of 24 with 0.5 M LiTFSI for a reaction time of 1 hour and without LiTFSI for 1 and 24 hours; H_2O : LiI of 134 with 0.5 M LiTFSI after a reaction time of 1 and 48 hours. Some unidentified signals were labelled by a star sign. Two peaks from the $LiOH{\cdot}H_2O$ phase shifted (838 cm^{-1} shifted to 829 cm^{-1} and 3566 cm^{-1} shifted to 3691 cm^{-1}), which could be related to the formation of some intermediate states, which requires further studies.

at 2.2 V_{Li} for cells with LiI, but no significant changes were noted for 2.7 V_{Li} (Fig. 8a). For galvanostatic tests, higher discharge voltages were found for electrodes in electrolytes with LiI and 1000 ppm H_2O (Fig. 8b), which is in agreement with the observation of Burke *et al.*[38] Here we propose that the higher discharge voltage over the entire capacity came from the following processes: (i) first a classical electrochemical 2e$^-$ O_2 reduction to form LiO_2/Li_2O_2, (ii) followed by a chemical reaction with water to form LiOH and H_2O_2, during which the iodide ions act as a catalyst, (iii) oxidation of I^- by H_2O_2 to form I_3^- and (iv) electrochemical reduction of I_3^- to I^- on the carbon electrode as depicted in Fig. 7b. The higher discharge potential in the presence of LiI and 1000 ppm H_2O (H_2O:LiI 0.48) can come from the fact that the I^-/I_3^- redox potential is centred at $\sim$3.0 V_{Li}. The proposed mechanism could give rise to an apparent 4-electron reduction of oxygen proposed by Burke *et al.*[38] Considering that 1000 ppm of H_2O in 0.15 ml of electrolyte accounted for 0.8 μmol of H_2O and 4000 mA h g^{-1} corresponded to 0.4 μmol of Li_2O_2 in our experiments, all produced Li_2O_2 can be converted to LiOH with 0.1 M LiI added using the proposed mechanism ($Li_2O_2 + 2H_2O + 3I^- + 2Li^+ \leftrightarrow I_3^- + 4LiOH$). The observation of a 2.8 V_{Li} plateau (Fig. 8b) might be assigned to the reduction of I_3^-[26,35] resulting from I^- being oxidized upon exposure to CNTs having an open circuit voltage of $\sim$3.2 V_{Li} in the LiTFSI-only electrolyte, which is higher than the equilibrium potential of I^-/I_3^- ($\sim$3.0 V_{Li}). This hypothesis is supported by the observation that upon addition

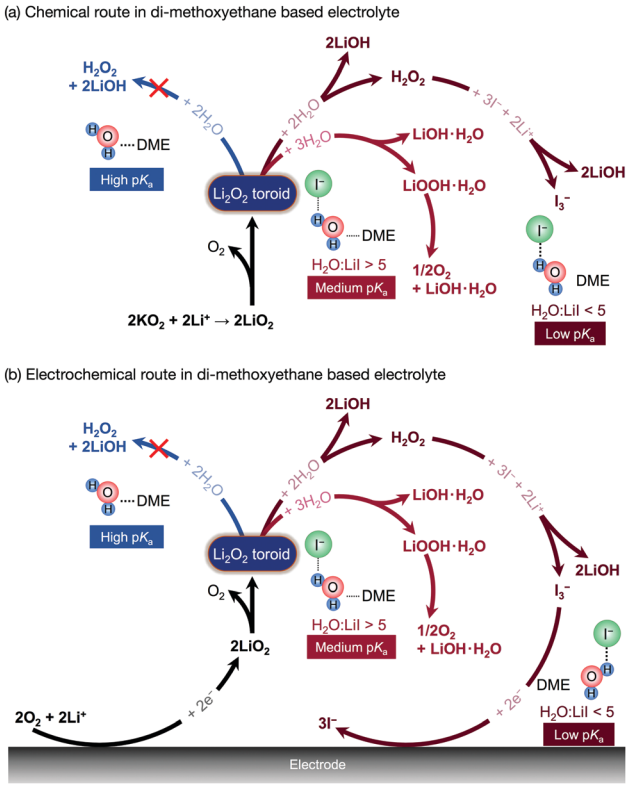

Fig. 7 The schematic of the Li–oxygen discharge process in the presence of H_2O and LiI in DME based electrolyte: (a) chemical route by mixing KO_2 with electrolyte containing Li^+ cations and (b) electrochemical route by discharging the Li–O_2 battery.

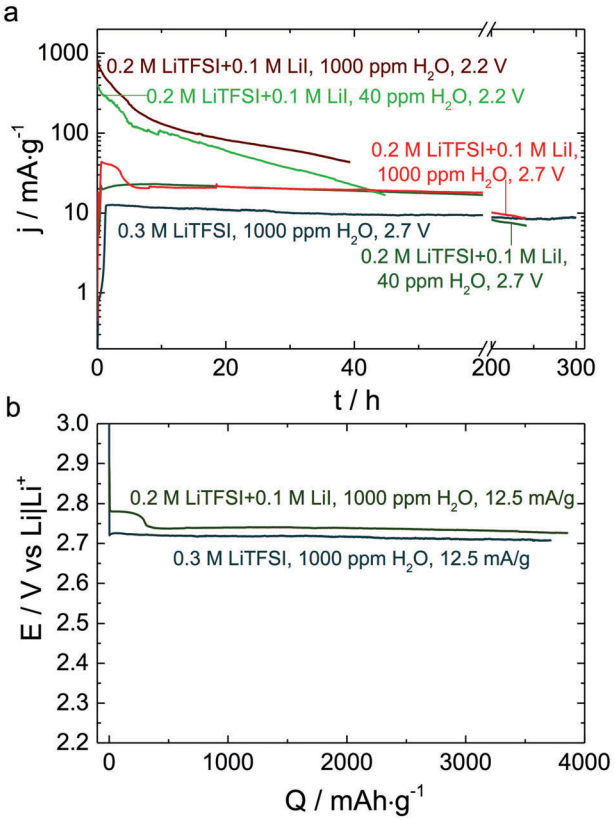

Fig. 8 (a) Potentiostatic and (b) galvanostatic discharge (12.5 mA g^{-1}) of Li/O_2 cells with CNTs (~1.6 mg) for the oxygen electrode, in 0.2/0.3 M LiTFSI solution in DME with and without addition of 0.1 M LiI and 1000 ppm H_2O (H_2O:LiI 0.48). The time of discharge varied from 2 to 14 days depending on the applied overvoltage.

of the electrolyte over the CNT electrode, a bright yellow coloration of the separator was observed, indicating the presence of I_3^- before discharge.

Adding 1000 ppm of H_2O in the absence of LiI produced only Li_2O_2 as revealed by XRD for electrodes discharged with galvanostatic and potentiostatic methods (Fig. 9), which is in agreement with previous work.[67] Under these conditions, large Li_2O_2 toroids (0.5 μm) were observed (Fig. 10a and b), which is characteristic for Li_2O_2 formed at high discharge potentials *via* disproportionation of soluble LiO_2.[2,10,41,45,55] In agreement with our findings in Fig. 1–3, Li_2O_2 was formed instead of LiOH even in the presence of strong oxidants such as LiO_2 and Li_2O_2, suggesting insignificant deprotonation of H_2O. With the addition of LiI, while only Li_2O_2 was detected at 40 ppm H_2O at both 2.7 and 2.2 V_{Li}, while a mixture of Li_2O_2 and LiOH was found with 1000 ppm H_2O (Fig. 9). It is worth noting that LiOH was found as the major phase upon discharge at 2.7 V_{Li} with 1000 ppm H_2O while Li_2O_2 was the major phase with LiOH as the minor at 2.2 V_{Li}, as shown in Fig. 9. The morphologies of Li_2O_2 were found to change from toroids to conformal coatings from 2.7 to 2.2 V_{Li} for 40 ppm H_2O with LiI (Fig. 10c and d), consistent with similar changes in 0.1 M $LiClO_4$ solution in either DMSO or DME solvent from our previous work.[41] Star-shaped particles (>1000 nm), characteristic of LiOH,[68] and thin-layer coatings over the CNT surfaces were found for electrodes discharged with LiI and 1000 ppm H_2O (Fig. 10e and f). Interestingly, less LiOH was found at 2.2 V_{Li} (1000 ppm and LiI) relative to 2.7 V_{Li}. The formation of LiOH results from the high reactivity of Li_2O_2 formed predominantly from disproportionation of LiO_2 at 2.7 V_{Li}, having small clusters of LiO_2 and Li_2O_2[54,55] as well as Li_2O_2 with superoxide-like surfaces.[10] At 2.2 V_{Li} there is a larger driving force for Li_2O_2 formation from direct 2e$^-$ transfer to O_2, rather than LiO_2 disproportion,[41] resulting in Li_2O_2 with less surface area and fewer LiO_2 clusters and/or less superoxide-like surfaces to deprotonate H_2O. Furthermore, the discharge time was much shorter at 2.2 V (~2 days) as compared to samples discharged at slow rate (~10 days), giving less time for Li_2O_2 to deprotonate H_2O. Therefore, adding LiI in Li–O_2 batteries would promote the formation of LiOH by irreversible deprotonation of H_2O and the electrolyte solvents.[38] The formation of LiOH instead of Li_2O_2 would lower the Faradaic and voltage efficiency and shorten the Li–O_2 battery cycle life, as shown by increased overpotentials during cycling as reported by Kwak *et al.*[26]

Upon washing the discharged electrodes with DME, we observed coloration of the solution resulting from I_3^- species, which was confirmed by UV-Vis (Fig. S17, ESI†). Unfortunately, the quantification of I^-/I_3^- concentration in the cell electrolyte did not yield further information as the produced I_3^- species can be either electrochemically reduced during discharge or

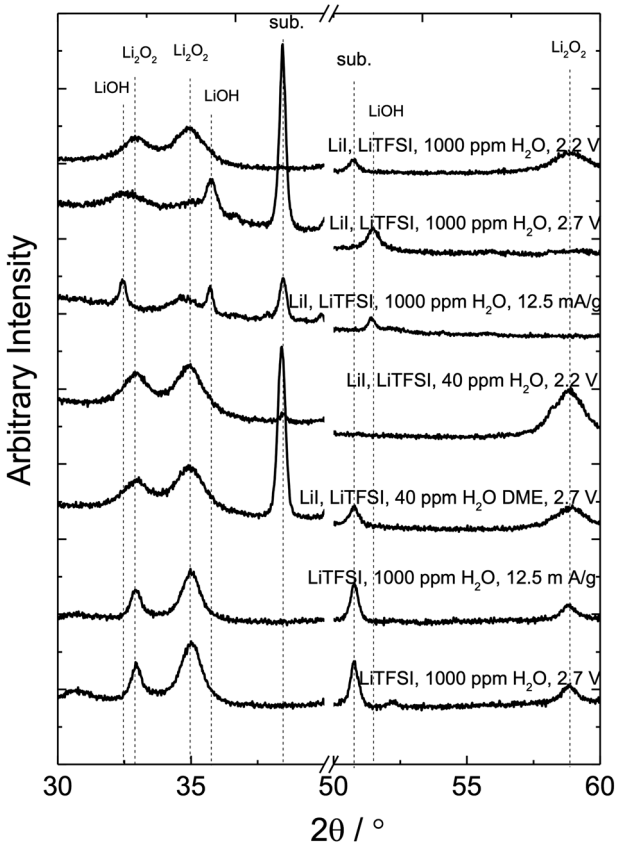

Fig. 9 XRD patterns of the CNT discharged electrodes at different conditions: 0.3 M LiTFSI in DME with 1000 ppm of H_2O discharged at 2.7 V_{Li} – dark blue and 12.5 mA g^{-1} – bright blue; 0.2 M LiTFSI + 0.1 M LiI in DME with 40 ppm of H_2O (H_2O:LiI 0.02) discharged at 2.7 V_{Li} – dark red and 2.2 V_{Li} – bright red; 0.2 M LiTFSI + 0.1 M LiI in DME with 1000 ppm of H_2O (H_2O:LiI 0.48) discharged at 2.7 V_{Li} – dark green, 12.5 mA g^{-1} – bright green and 2.2 V_{Li} – light green. Black dashed lines indicate the position of Li_2O_2, LiOH and substrate (sub.) peaks.

reduced chemically with metallic lithium (negative electrode) while the battery is discharging and/or resting.

Our results clearly indicate that in the presence of H_2O and LiI, the major discharge phase is either LiOH and I_3^- or LiOH·H_2O. The formation of I_3^- from oxidation of I^- is not harmful to the battery. However, the formation of LiOH is detrimental to battery performance as it passivates the active surface for Li_2O_2 formation. Although some reports[32,35] mention that LiOH/LiOH·H_2O can be oxidized by either I_3^- or I_2, ambiguity exists on this aspect and needs further investigation, especially for high water levels and H_2O : LiI ratios. Nevertheless, at low water levels and low H_2O : LiI ratios, Burke *et al.*[38] have shown that LiOH oxidation is unlikely as it can react with I_2 to form $LiIO_3$, which is not electroactive. Therefore, for aprotic electrolytes, H_2O contamination should be avoided or strategies to reduce LiOH formation should be explored.

Conclusions

We show that the chemical disproportionation by mixing lithium salts with KO_2 in DME-based electrolytes with and without added H_2O results in the formation of mostly Li_2O_2 without LiI. On the other hand, adding LiI and H_2O to the DME-based electrolytes that have low H_2O : LiI ratios (<5) renders LiOH as the major product from the disproportionation, which is accompanied by oxidation of I^- to I_3^-. Similar observations have been noted upon Li–O_2 battery discharge at high discharge voltages to those from the disproportionation reaction. The formation of LiOH instead of Li_2O_2 with the addition of LiI and H_2O can be attributed to the greater acidity of water associated with strong I^-–H_2O interactions at low H_2O : LiI ratios (<5), which promotes the formation of LiOH and H_2O_2 from the reaction between H_2O and $Li_2O_{2S\text{-}LiO_2}$

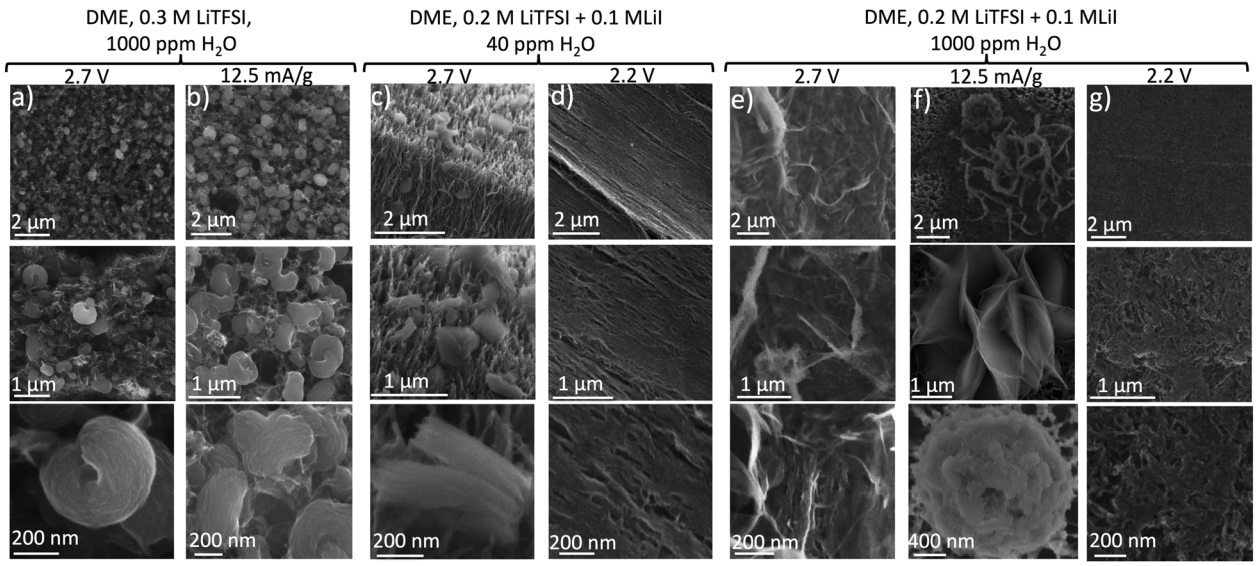

Fig. 10 SEM images of the CNT discharged electrodes. 0.3 M LiTFSI in DME with 1000 ppm of H_2O discharged at (a) 2.7 V_{Li} and (b) 12.5 mA g^{-1}; 0.2 M LiTFSI + 0.1 M LiI in DME with 40 ppm of H_2O (H_2O : LiI 0.02) discharged at (c) 2.7 V_{Li} and (d) 2.2 V_{Li}; 0.2 M LiTFSI + 0.1 M LiI in DME with 1000 ppm of H_2O (H_2O:LiI 0.48) discharged at (e) 2.7 V_{Li}, (f) 12.5 mA g^{-1} and (g) 2.2 V_{Li}.

produced by disproportionation. In addition, shifting the equilibrium for the reaction between Li_2O_2 and H_2O (such as $Li_2O_2 + 2H_2O \rightleftharpoons H_2O_2 + 2LiOH$) to the right with continuous consumption of H_2O_2 by lithium iodide ($3LiI + H_2O_2 \rightleftharpoons LiI_3 + 2LiOH$) can lead to more LiOH. In contrast, at high H_2O : LiI ratios (12, 24 and 134), lower H_2O acidity can lead to the formation of $LiOOH{\cdot}H_2O$ instead of LiOH and H_2O_2. $LiOOH{\cdot}H_2O$ can disproportionate to form $LiOH{\cdot}H_2O$ without the formation of H_2O_2 and corresponding oxidation of I^- to I_3^-. These findings show that LiI mediates the deprotonation of water by Li_2O_2 species in a DME-based electrolyte, resulting in the formation of LiOH or $LiOH{\cdot}H_2O$, which can hamper the cycle life of Li–air batteries. Therefore, these findings indicate that LiI might not be a suitable redox mediator to promote the reversibility and cycle life of lithium–air batteries. Further work on redox mediators and electrolytes should therefore focus on strategies to suppress parasitic pathways while still preserving their kinetic advantages for Li–O_2 electrochemistry.

Acknowledgements

The work was supported in part by Toyota Motor Europe and the Skoltech Center for Electrochemical Energy Storage. SEM imaging and XRD measurements were performed at the MRSEC Shared Experimental Facilities at MIT, supported by the National Science Foundation under award number DMR-1419807. CVA was supported by the US Department of Defense through the National Defense Science and Engineering Graduate (NDSEG) Fellowship and the Alfred P. Sloan Foundation's Minority PhD Program. We also would like to thank Shuting Feng for discussion.

Notes and references

1 P. G. Bruce, S. A. Freunberger, L. J. Hardwick and J.-M. Tarascon, *Nat. Mater.*, 2011, **11**, 19–29.
2 Y.-C. Lu, B. M. Gallant, D. G. Kwabi, J. R. Harding, R. R. Mitchell, M. S. Whittingham and Y. Shao-Horn, *Energy Environ. Sci.*, 2013, **6**, 750–768.
3 P. Albertus, G. Girishkumar, B. McCloskey, R. S. Sanchez-Carrera, B. Kozinsky, J. Christensen and A. C. Luntz, *J. Electrochem. Soc.*, 2011, **158**, A343–A351.
4 K. B. Knudsen, A. C. Luntz, S. H. Jensen, T. Vegge and J. Hjelm, *J. Phys. Chem. C*, 2015, **119**, 28292–28299.
5 A. A. Franco and K. H. Xue, *ECS J. Solid State Sci. Technol.*, 2013, **2**, M3084–M3100.
6 Y. Li, J. Wang, X. Li, D. Geng, M. N. Banis, Y. Tang, D. Wang, R. Li, T.-K. Sham and X. Sun, *J. Mater. Chem.*, 2012, **22**, 20170–20174.
7 B. Horstmann, B. Gallant, R. Mitchell, W. G. Bessler, Y. Shao-Horn and M. Z. Bazant, *J. Phys. Chem. Lett.*, 2013, **4**, 4217–4222.
8 J.-J. Xu, Z.-L. Wang, D. Xu, L.-L. Zhang and X.-B. Zhang, *Nat. Commun.*, 2013, **4**, 1–10.
9 J.-J. Xu, Z.-W. Chang, Y. Wang, D.-P. Liu, Y. Zhang and X.-B. Zhang, *Adv. Mater.*, 2016, **28**, 9620–9628.
10 B. M. Gallant, D. G. Kwabi, R. R. Mitchell, J. Zhou, C. V. Thompson and Y. Shao-Horn, *Energy Environ. Sci.*, 2013, **6**, 2518–2528.
11 G. Girishkumar, B. McCloskey, A. C. Luntz, S. Swanson and W. Wilcke, *J. Phys. Chem. Lett.*, 2010, **1**, 2193–2203.
12 R. Black, B. Adams and L. F. Nazar, *Adv. Energy Mater.*, 2012, **2**, 801–815.
13 Y.-C. Lu, H. A. Gasteiger and Y. Shao-Horn, *J. Am. Chem. Soc.*, 2011, **133**, 19048–19051.
14 F. Cheng and J. Chen, *Chem. Soc. Rev.*, 2012, **41**, 2172–2192.
15 Z.-L. Wang, D. Xu, J.-J. Xu and X.-B. Zhang, *Chem. Soc. Rev.*, 2014, **43**, 7746–7786.
16 J.-J. Xu, D. Xu, Z.-L. Wang, H.-G. Wang, L.-L. Zhang and X.-B. Zhang, *Angew. Chem., Int. Ed.*, 2013, **52**, 3887–3890.
17 K. P. C. Yao, M. Risch, S. Y. Sayed, Y.-L. Lee, J. R. Harding, A. Grimaud, N. Pour, Z. Xu, J. Zhou, A. Mansour, F. Barde and Y. Shao-Horn, *Energy Environ. Sci.*, 2015, **8**, 2417–2426.
18 Y.-B. Yin, J.-J. Xu, Q.-C. Liu and X.-B. Zhang, *Adv. Mater.*, 2016, **28**, 7494–7500.
19 L. Li and A. Manthiram, *Adv. Energy Mater.*, 2014, **4**, 1301795.
20 J. Shui, Y. Lin, J. W. Connell, J. Xu, X. Fan and L. Dai, *ACS Energy Lett.*, 2016, **1**, 260–265.
21 Y.-C. Lu, Z. Xu, H. A. Gasteiger, S. Chen, K. Hamad-Schifferli and Y. Shao-Horn, *J. Am. Chem. Soc.*, 2010, **132**, 12170–12171.
22 Z. Cui, L. Li, A. Manthiram and J. B. Goodenough, *J. Am. Chem. Soc.*, 2015, **137**, 7278–7281.
23 D. Sun, Y. Shen, W. Zhang, L. Yu, Z. Q. Yi, W. Yin, D. Wang, Y. H. Huang, J. Wang, D. L. Wang and J. B. Goodenough, *J. Am. Chem. Soc.*, 2014, **136**, 8941–8946.
24 D. Kundu, R. Black, B. Adams and L. F. Nazar, *ACS Cent. Sci.*, 2015, **1**, 510–515.
25 T. Zhang, K. M. Liao, P. He and H. S. Zhou, *Energy Environ. Sci.*, 2016, **9**, 1024–1030.
26 W. J. Kwak, D. Hirshberg, D. Sharon, H. J. Shin, M. Afri, J. B. Park, A. Garsuch, F. F. Chesneau, A. A. Frimer, D. Aurbach and Y. K. Sun, *J. Mater. Chem. A*, 2015, **3**, 8855–8864.
27 Y. H. Chen, S. A. Freunberger, Z. Q. Peng, O. Fontaine and P. G. Bruce, *Nat. Chem.*, 2013, **5**, 489–494.
28 W. R. Torres, S. E. Herrera, A. Y. Tesio, M. del Pozo and E. J. Calvo, *Electrochim. Acta*, 2015, **182**, 1118–1123.
29 B. J. Bergner, A. Schurmann, K. Peppler, A. Garsuch and J. Janek, *J. Am. Chem. Soc.*, 2014, **136**, 15054–15064.
30 B. J. Bergner, M. R. Busche, R. Pinedo, B. B. Berkes, D. Schroder and J. Janek, *ACS Appl. Mater. Interfaces*, 2016, **8**, 7756–7765.
31 N. N. Feng, P. He and H. S. Zhou, *ChemSusChem*, 2015, **8**, 600–602.
32 Y. G. Zhu, Q. Liu, Y. Rong, H. Chen, J. Yang, C. Jia, L.-J. Yu, A. Karton, Y. Ren, X. Xu, S. Adams and Q. Wang, *Nat. Commun.*, 2017, **8**, 1–8.
33 W.-J. Kwak, D. Hirshberg, D. Sharon, M. Afri, A. A. Frimer, H.-G. Jung, D. Aurbach and Y.-K. Sun, *Energy Environ. Sci.*, 2016, **9**, 2334–2345.

34 H. D. Lim, H. Song, J. Kim, H. Gwon, Y. Bae, K. Y. Park, J. Hong, H. Kim, T. Kim, Y. H. Kim, X. Lepro, R. Ovalle-Robles, R. H. Baughman and K. Kang, *Angew. Chem., Int. Ed.*, 2014, **53**, 3926–3931.
35 T. Liu, M. Leskes, W. J. Yu, A. J. Moore, L. N. Zhou, P. M. Bayley, G. Kim and C. P. Grey, *Science*, 2015, **350**, 530–533.
36 Z. J. Liang and Y. C. Lu, *J. Am. Chem. Soc.*, 2016, **138**, 7574–7583.
37 X. Zeng, L. Leng, F. Liu, G. Wang, Y. Dong, L. Du, L. Liu and S. Liao, *Electrochim. Acta*, 2016, **200**, 231–238.
38 C. M. Burke, R. Black, I. R. Kochetkov, V. Giordani, D. Addison, L. F. Nazar and B. D. McCloskey, *ACS Energy Lett.*, 2016, 747–756.
39 Y. Shen, W. Zhang, S.-L. Chou and S.-X. Dou, *Science*, 2016, **352**, 667-a.
40 V. Viswanathan, V. Pande, K. M. Abraham, A. C. Luntz, B. D. McCloskey and D. Addison, *Science*, 2016, **352**, 667-c.
41 D. G. Kwabi, M. Tulodziecki, N. Pour, D. M. Itkis, C. V. Thompson and Y. Shao-Horn, *J. Phys. Chem. Lett.*, 2016, **7**, 1204–1212.
42 K. P. C. Yao, D. G. Kwabi, R. A. Quinlan, A. N. Mansour, A. Grimaud, Y. L. Lee, Y. C. Lu and Y. Shao-Horn, *J. Electrochem. Soc.*, 2013, **160**, A824–A831.
43 P. J. Brandhuber and G. Korshin, *Methods for the detection of residual concentrations of hydrogen peroxide in advanced oxidation process*, Watereuse Foundation, Alexandria, 2009.
44 B. M. Gallant, R. R. Mitchell, D. G. Kwabi, J. G. Zhou, L. Zuin, C. V. Thompson and Y. Shao-Horn, *J. Phys. Chem. C*, 2012, **116**, 20800–20805.
45 R. R. Mitchell, B. M. Gallant, Y. Shao-Horn and C. V. Thompson, *J. Phys. Chem. Lett.*, 2013, **4**, 1060–1064.
46 D. G. Kwabi, T. P. Batcho, S. Feng, L. Giordano, C. V. Thompson and Y. Shao-Horn, *Phys. Chem. Chem. Phys.*, 2016, **18**, 24944–24953.
47 M. C. Milenkovic and D. R. Stanisavljev, *Russ. J. Phys. Chem. A*, 2011, **85**, 2279–2282.
48 B. D. Adams, R. Black, Z. Williams, R. Fernandes, M. Cuisinier, E. J. Berg, P. Novak, G. K. Murphy and L. F. Nazar, *Adv. Energy Mater.*, 2015, **5**, 1400867.
49 V. S. Bryantsev and F. Faglioni, *J. Phys. Chem. A*, 2012, **116**, 7128–7138.
50 S. Di Tommaso, P. Rotureau, O. Crescenzi and C. Adamo, *Phys. Chem. Chem. Phys.*, 2011, **13**, 14636–14645.
51 N. Mahne, B. Schafzahl, C. Leypold, M. Leypold, S. Grumm, A. Leitgeb, G. A. Strohmeier, M. Wilkening, O. Fontaine, D. Kramer, C. Slugovc, S. M. Borisov and S. A. Freunberger, *Nat. Energy*, 2017, **2**, 17036.
52 Y. Che, M. Tsushima, F. Matsumoto, T. Okajima, K. Tokuda and T. Ohsaka, *J. Phys. Chem.*, 1996, **100**, 20134–20137.
53 M. Hayyan, M. A. Hashim and I. M. AlNashef, *Chem. Rev.*, 2016, **116**, 3029–3085.
54 T. K. Zakharchenko, A. Y. Kozmenkova, D. M. Itkis and E. A. Goodilin, *Beilstein J. Nanotechnol.*, 2013, **4**, 758–762.
55 Y. Zhang, X. Zhang, J. Wang, W. C. McKee, Y. Xu and Z. Peng, *J. Phys. Chem. C*, 2016, **120**, 3690–3698.
56 D. Sharon, V. Etacheri, A. Garsuch, M. Afri, A. A. Frimer and D. Aurbach, *J. Phys. Chem. Lett.*, 2013, **4**, 127–131.
57 D. Sharon, M. Afri, M. Noked, A. Garsuch, A. A. Frimer and D. Aurbach, *J. Phys. Chem. Lett.*, 2013, **4**, 3115–3119.
58 B. D. McCloskey, A. Valery, A. C. Luntz, S. R. Gowda, G. M. Wallraff, J. M. Garcia, T. Mori and L. E. Krupp, *J. Phys. Chem. Lett.*, 2013, **4**, 2989–2993.
59 K. U. Schwenke, M. Metzger, T. Restle, M. Piana and H. A. Gasteiger, *J. Electrochem. Soc.*, 2015, **162**, A573–A584.
60 S. Chowdhuri and A. Chandra, *J. Phys. Chem. B*, 2006, **110**, 9674–9680.
61 A. Karmakar and A. Chandra, *J. Phys. Chem. B*, 2015, **119**, 8561–8572.
62 M. Forsyth and D. R. MacFarlane, *J. Phys. Chem.*, 1990, **94**, 6889–6893.
63 M. L. Hair and W. Hertl, *J. Phys. Chem.*, 1970, **74**, 91–94.
64 D. Pines, S. Keinan, P. M. Kiefer, J. T. Hynes and E. Pines, *J. Phys. Chem. B*, 2015, **119**, 9278–9286.
65 E. E. Platero, M. P. Mentruit, C. O. Areán and A. Zecchina, *J. Catal.*, 1996, **162**, 268–276.
66 A. Tongraar, S. Hannongbua and B. M. Rode, *J. Phys. Chem. A*, 2010, **114**, 4334–4339.
67 N. B. Aetukuri, B. D. McCloskey, J. M. Garcia, L. E. Krupp, V. Viswanathan and A. C. Luntz, *Nat. Chem.*, 2015, **7**, 50–56.
68 D. G. Kwabi, T. P. Batcho, C. V. Amanchukwu, N. Ortiz-Vitoriano, P. Hammond, C. V. Thompson and Y. Shao-Horn, *J. Phys. Chem. Lett.*, 2014, **5**, 2850–2856.

